Simulation of a Dust Impact Time-of-flight Dust Particle Sensor

Igor Piyakov
Institute of space instrument engineering
Samara National Research University
Samara, Russia
igor_piyakov@ssau.ru

Dmitry Rodin
Institute of space instrument engineering
Samara National Research University
Samara, Russia
rodin@ssau.ru

Marina Rodina
Institute of space instrument engineering
Samara National Research University
Samara, Russia
m.a.rodina@yandex.ru

Alexey Telegin
Institute of space instrument engineering
Samara National Research University
Samara, Russia
talex85@mail.ru

***Abstract*—One-dimensional and two-dimensional axisymmetric models of a dust impact time-of-flight dust particle sensor for analysis of the chemical composition of micrometeoroids and particles of space debris are considered. The results of calculating the design parameters and functional characteristics of the sensor are presented. The algorithm of the program for modelling mass spectra is described. Model mass spectra obtained for the axial case in the one-dimensional approximation, as well as for the two-dimensional case and various coordinates of the impact interaction, are presented. The comparison of model spectra with experimental data obtained at the electrodynamic accelerator of dust particles is given.**

Keywords—dust-impact sensor, micrometeorite, mass-spectrometr

I. INTRODUCTION

Currently, more and more attention is paid to the problem of space debris, which is associated both with an increase in the terms of active existence of spacecrafts, and with an increasing number of anthropogenic origin space debris. Micrometeoroids and anthropogenic dust particles are one of the main factors in outer space, which, along with various emissions and streams of charged particles, cause premature degradation of structural elements of the spacecraft [1, 2], which means that they can lead to a deterioration of its functional characteristics, or failure. Various methods can be used to analyze the properties of dust particle flows, such as aerogel-based traps, non-contact optical measurers, impact ionization sensors [3, 4]. But the greatest amount of information on the physical and chemical properties of a projectile particle can only be obtained by using a mass-spectrometric type dust impact time-of-flight sensor. Such an analyzer makes it possible to investigate single fast-transient events and evaluate not only the chemical composition of a particle, but also its charge, velocity vector and, indirectly, mass.

The principle of operation of such analyzers [5 - 8] is based on impact ionization of the material of the impact particle, followed by acceleration of ions by the electric field and measurement of their transit time. High resolution can be achieved by ensuring a minimum fluctuation in the transit time of ions of the same mass inside the ion packet, which is ensured by focusing the ions in time and space. The development of such devices is always fraught with great difficulties, as having high resolution they are subject to internally conflicting requirements for increasing the active area of the target and increasing the ion collection coefficient. The solution to this problem requires a large amount of mathematical modeling, as well as experimental studies confirming the correct choice of design parameters. Therefore, verification of the simulation results allows to reduce the amount of experimental research required and speed up the process of developing new devices.

II. STATEMENT OF THE PROBLEM

The principle of the device operation is presented in the ion optical diagram (Fig. 1).

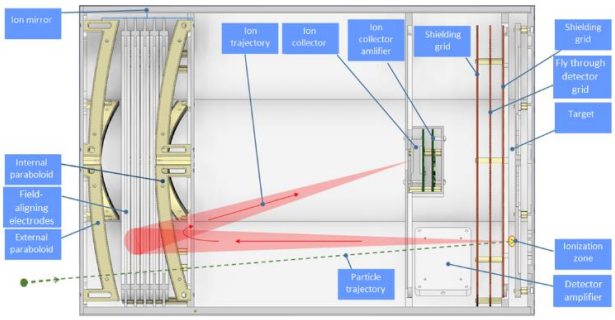

Fig. 1. Ion optical diagram of scientific equipment SPECTR.

At the initial moment, the dust particle hits the target and transforms into a cloud of weakly ionized gas, consisting of ions of the particle material and the target. An electrical signal is formed during the flight through the detector grid, along which the recording of a data frame containing information from the ion receiver begins. Under the influence of an electric field formed by the potential difference of the target and the shielding grid, the ion cloud accelerates in the direction of the ion mirror. The ion mirror is made in the form of five field-aligning electrodes and four parabolic grids, the focal point of which coincides with the receiver of ions. After the turn, the ions enter the receiver and the signal from the amplifier of the ion receiver enters the microcontroller module. The design described in [9] was changed as follows: in order to increase the ion collection coefficient, one of the ion mirrors was removed in order to increase the resolution, the accelerating voltage was increased to 1125 V, an additional grid after the parabolic reflector serves to guarantee the reflection of all ions in side of the receiver. The schematic diagram of the target, electrodes and receiver, as well as the potentials distribution, is shown in Fig. 2.

CEUR-WS.org/Vol-2667/paper16.pdf

Copyright © 2020 for this paper by its authors.
Use permitted under Creative Commons License Attribution 4.0 International (CC BY 4.0)

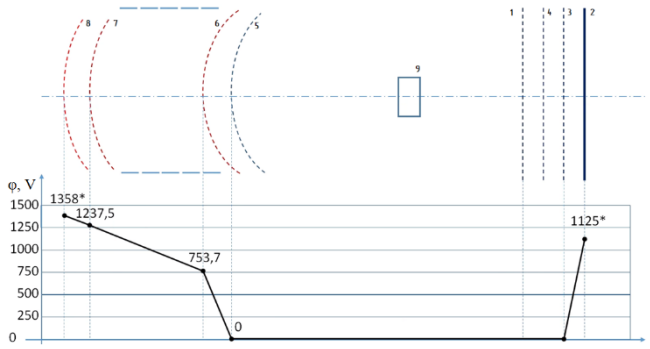

Fig. 2. Dust impact mass-spectrometer with parabolic reflector (2 – target; 1,3 – shielding grids, grounded; 4 – fly-through detector grid; 5, 6, 7, 8 – parabolic ion mirror grids; 9 – receiver casing, grounded).

III. CALCULATION OF THE PARAMETERS OF THE SENSOR

A. *One-dimensional model*

We write an expression that determines the time of flight of a particle of mass m and charge q with an initial energy ΔU:

$$T = \left(\frac{m}{2q}\right)^{1/2} \left\{\frac{2L_1}{U_1}\left[\sqrt{\Delta U + U_1(1+n)} - \sqrt{\Delta U}\right] + \right.$$
$$+\frac{4L_3}{k_1U_1}\left[\sqrt{\Delta U + U_1} - \sqrt{\Delta U + U_1(1-k_1)}\right] +$$
$$\left. +\frac{4L_4}{k_2U_1}\sqrt{\Delta U + U_1(1-k_1)} + L_{\text{fl}}(\Delta U + U_1)^{-1/2}\right.$$

Further, we write through the coefficients

$$T = \left(\frac{m}{2q}\right)^{1/2} \left[C_1\sqrt{\Delta U} + C_2\sqrt{\Delta U + U_1} + \right.$$
$$\left. +C_3\sqrt{\Delta U + U_1(1-k_1)} + C_4(\Delta U + U_1)^{-1/2}\right] C_1 = -\frac{2L_1}{U_1};$$

$$C_2 = \frac{2L_1}{U_1} + \frac{4L_3}{k_1U_1};$$

$$C_3 = -\frac{4L_3}{k_1U_1} + \frac{4L_4}{k_2U_1};$$

$$C_4 = L_{\text{fl}}.$$

In order for the initial energy spread of ions not to have a negative effect on the time focusing of ions in the mass spectrometric path, the first two derivatives of the expression must be equal to zero when the ions energy spread tends to zero

$$\begin{cases} \left(\dfrac{\mathrm{d}T}{\mathrm{d}U}\right)_{U=U_0} = 0; \\ \left(\dfrac{\mathrm{d}^2T}{\mathrm{d}U^2}\right)_{U=U_0} = 0. \end{cases}$$

Sometimes it requires the three derivatives to be equal to zero. In this case we deal with third-order focusing.

In practice, it is not always possible to solve such a system of equations. So, if we look at the first derivative of the expression, the term $C_1\sqrt{\Delta U}$ turns into $L_1\left(C_1\sqrt{\Delta U}\right)^{-1}$ after substitution and differentiation. In condition when ΔU tends to zero, the derivative tends to infinity. By tending ΔU to very small values, we obtain a solution that cannot be realized constructively: the sizes L_1 and L_2 will be very small (L_1 tends to zero, and the value of L_2 is of the order of mm).

Therefore, in practice, a different approach can be used: it is possible to zero out the difference in the time of flight of ions with zero energy and with a boundary energy located in the middle of the energy spectra with structurally fixed feasible sizes

$$\Delta T = \left(\frac{m}{2q}\right)^{1/2} \left[C_0 - C_1\sqrt{\Delta U} - C_2\sqrt{\Delta U + U_1} - \right.$$
$$\left. - C_3\sqrt{\Delta U + U_1(1-k_1)} - C_4(\Delta U + U_1)^{-1/2}\right],$$

where

$$C_0 = \frac{1}{\sqrt{U_1}}\left[2L_1 + L_{\text{fl}} + \frac{4L_3\left(1-\sqrt{1-k_1}\right)}{k_1} + \frac{4L_4\sqrt{1-k_1}}{k_2}\right];$$

$\Delta T = 0$ for $U = U_{\text{const}}$.

Fig. 3 shows a comparison of the device resolution dependence on energy calculated in two ways. On the left, the characteristics obtained for exact sizes are shown, on the right, the characteristics obtained for a device with an 5% linear dimensions error, which is permissible for electrodes and grids as single piece produced parts. The peak on the graph corresponds to the selected boundary energy, at which the area under the resolution curve is maximum in the region of interest of the energy spectra.

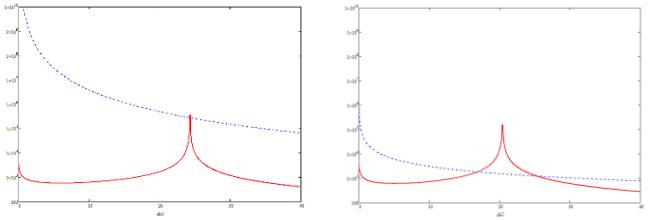

Fig. 3. Comparison of the dependence of the device resolution on energy calculated in two ways.

Although the calculation through derivatives makes it possible to obtain very high resolution values, in practice, even with small deviations from ideal sizes (not to mention constructive unrealizability), the resolution of such a device quickly decreases.

The calculation result for the axial case is the distance between the grids and the voltage at the electrodes, however, the dimensions along the radial coordinate and the approach to spatial focusing require volume modeling.

B. *Two-dimensional axisymmetric model*

The initial data obtained as a result of a one-dimensional calculation are insufficient for a complete design, two parameters are also necessary - the target diameter and the distance to the ion receiver. Based on our previous prototyping experience, we selected a target diameter of 24 cm. The position of the ion detector, as well as the focal length of a parabolic ion mirror, was determined by the design and ease of manufacture.

The verification of the calculation results was carried out in two stages. At the first stage, a simulation of the structure was carried out with length deviations of the field-free path from the nominal one, the simulation results are shown in Table I. It can be seen that the length of field-free path, equal to 518 mm, is optimal for the given design.

At the second stage, after confirming the correct choice for the axial location of the interaction point, collision spectra were simulated for different radial coordinates. The results of calculating the collection coefficient and the deviation of the time of flight are shown in Table II.

TABLE I. THE RESOLUTION OF THE DEVICE DEPENDING ON THE INITIAL ION ENERGY AND LENGTH OF THE FIELD-FREE AREA

Length of the Field-Free Area, mm	**Initial Ion Energy, eV**		
	ΔU = 1	***ΔU = 2***	***ΔU = 4***
L_2 **= 511**	382	382	164
L_2 **= 518**	386	386	165
L_2 **= 525**	333	259	163

TABLE II. COEFFICIENTS OF COLLECTION AND DEVIATION OF THE TIME OF FLIGHT OF IONS DEPENDING ON THE INITIAL ION ENERGY FOR A FOCAL LENGTH OF 22 CM

Characteristics	**Initial Ion Energy, eV**		
	ΔU = 4	***ΔU = 2***	***ΔU = 1***
$K_{collect}$	0.21	0.32	0.39
δT_{fl} **(S)**	$1.48 \cdot 10^{-7}$	$1.50 \cdot 10^{-7}$	$1.49 \cdot 10^{-7}$

IV. CALCULATION ALGORITHM

To analyze the two-dimensional case, we used the CPU implementation of the algorithm described in detail in [9]. To calculate the ion trajectories, we used a triangular irregular grid of field values containing information about the electrodes and domains of the calculation volume. The iterative calculation was carried out by the fourth-order Runge-Kutta method, special attention was paid to the algorithm for searching a new triangle when the particle leaves the boundaries of the current one.

Approximately, the initial temperature of the plasmoid was determined according to the formula:

$$T_0 = 0.1 \cdot \left(V_0 \left(1 + \sqrt{\frac{\rho_i}{\rho_t}} \right)^{-1} \right),$$

where V_0 is the microparticle speed, $\frac{\rho_i}{\rho_t}$ is the ratio of microparticle density to target density.

The distribution of ion velocities in a plasmoid, which is a multicomponent plasma depending on temperature, obeys the Maxwell distribution:

$$f_q(V) = \eta_j Q \sqrt{\frac{2m_j}{\pi k T_j}} \exp\left(-\frac{m_j V^2}{2kT_j} \right),$$

where Q is the total plasma charge, m_j is the mass of ions, k is the Boltzmann constant, T_j is the temperature, η_j is the fraction of j-type ions in the total plasma.

To generate a given probability distribution, the Box-Muller algorithm was used. To calculate the spectra, a module was written to calculate the number of ions that hit the receiver per unit time with a given sampling frequency (or the width of the time window).

The step-by-step algorithm of the program on a triangular grid does not differ sufficiently from the one described above, with the exception of the last paragraph.

1. Loading data on the computational grid with a field from a file.

2. File parsing: linking nodes, triangles, areas and field values.

3. Creating a Mesh object with a description of the relationships of nodes and triangles.

4. The formation of a model ion packet based on the given coordinates and the interaction speed.

5. Finding the current triangle for each ion.

6. Interpolation of the field at the location of each ion.

7. Calculation of the displacement of each ion over time dt.

8. Checking the location of the ion in the current triangle.

9. The recursive search for a new triangle.

10. Checking for ion loss or detection.

11. Repeat steps 6-10.

12. Upon reaching the maximum calculation time, stop and count the detected ions per unit time.

V. EXPERIMENTAL TESTING

Based on the calculation results, a prototype of the device was manufactured. The front view is shown in Fig. 4.

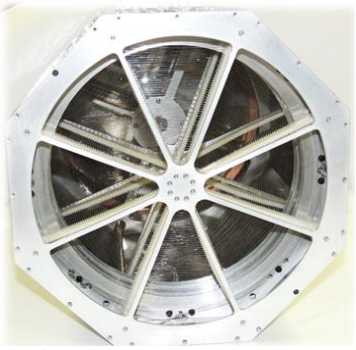

Fig. 4. Front view of the dust impact dust particle sensor: the grid, the target of the device and the particle detector input window.

During experimental testing at the dust particle accelerator [9, 10], the steel target was exposed to a flow of high-speed aluminum particles with speeds of up to 6 km / s. The simulation results with a typical spectrum containing mass lines Li (4.7 μs), N (6.7 μs), Al (9.15 μs), N2 (9.5 μs), K (11.2 μs) are shown in Fig. 5.

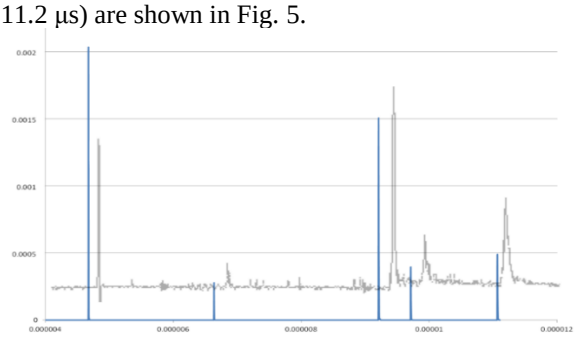

Fig. 5. Comparison of model and experimental spectra. For convenience, the experimental spectrum is shifted by 2.5 μ s to the right and up.

VI. CONCLUSION

The analytical calculation and two-dimensional modeling allowed to obtain a significant amount of information about the device operation and to select the optimal design parameters that can provide an increase in the collection coefficient and resolution with the same low weight-size parameters, which is almost impossible to obtain as a result of full-scale experimental testing.

The simulation results showed good convergence with the experimental results and confirmed the applicability of this approach to solve the design problems of more complex time-of-flight sensors.

REFERENCES

[1] N.D. Semkin, M.P. Kalaev and A.M. Telegin, "Multilayer film structures under the influence of micrometeoroids and space debris," Applied Physics, vol. 2, pp. 104-115, 2012.

[2] M.P. Kalaev, A.M. Telegin, K.E. Voronov, J. Lixiang and J. Jilong, "Investigation of optical glass characteristics under the influence of space factors," Computer Optics, vol. 43, no. 5, pp. 803-809, 2019. DOI: 10.18287/2412-6179-2019-43-5-803-809.

[3] L.S. Novikov, "The Effects of Particulate Matter of Natural and Artificial Origin on Spacecraft: A Training Manual," Moscow: University book, 2009, 104 p.

[4] W. Bauer, O. Romberg and C. Wiedemann, "Development of in-situ space debris detector," Advances in Space Research, vol. 54, pp. 1858-1869, 2014.

[5] N.A. Inogamov, "Collision of a micrometeoroid with an anode as an ion source for mass spectrometry," Soviet Technical Physics Letters, vol. 10, pp. 323-324, 1984.

[6] S.V. Zhitenev, N.A. Inogamov and A.B. Konstantinov, "Time-of-flight mass-spectrometer with dust-impact ion source," Journal of engineering physics, vol. 50, pp. 518-526, 1986.

[7] T.J. Ahrens, S.C. Gupta and G. Jyoti, "Mass spectrometer calibration of Cosmic Dust Analyzer," Journal of geophysical research, vol. 108, pp. 967-970, 2003.

[8] J.K. Hillier, F. Postberg, S. Sestak, "Impact ionization mass spectra of anorthite cosmic dust analogue particles," Journal of geophysical research, vol. 117, pp. 1-16, 2012.

[9] I.V. Piyakov, D.V. Rodin and M.A. Rodina, "Numerical simulation of the ion focusing process in a dust impact time of flight mass spectrometer," CEUR Workshop Proceedings, vol. 2212, pp. 152-157, 2018.

[10] A.V. Piyakov, D.V. Rodin, M.A. Rodina and A.M. Telegin, "Numerical simulation of motion of dust particles in an accelerator path," CEUR Workshop Proceedings, vol. 1902, pp. 55-61, 2017.